ACS OMEGA

http://pubs.acs.org/journal/acsodf

Article

UV−vis−IR Broad Spectral Photodetectors Based on VO_2−ZnO Nanocrystal Films

Danting Xu,[†] Xia Zhu,[†] Jiakun An, Gaoyu Chen, Jianchun Bao, and Xiangxing Xu*

Cite This: *ACS Omega* 2022, 7, 37078−37084

Read Online

ACCESS | Metrics & More | Article Recommendations | Supporting Information

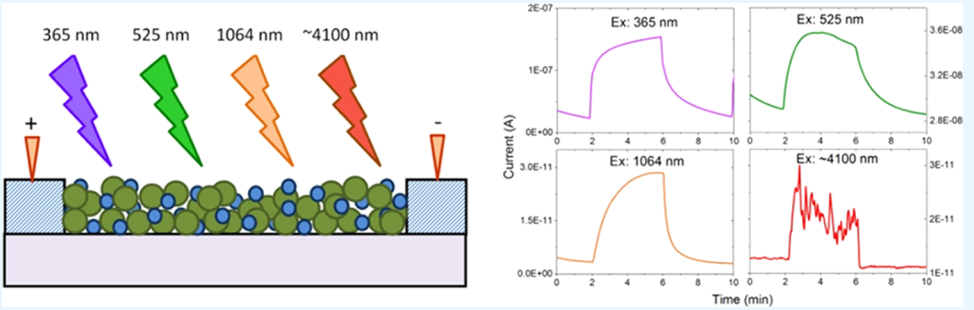

ABSTRACT: As a narrow band semiconductor at room temperature and a metallic material above ∼68 °C, functional VO_2 films are widely investigated for smart windows, whereas their potential for ultraviolet−visible−infrared (UV−vis−IR) broad spectral photodetectors has not been efficiently studied. In this report, photodetectors based on VO_2−ZnO nanocrystal composite films were prepared by nanocrystal-mist (NC-mist) deposition. An enhanced photodetection switching ratio was achieved covering the ultraviolet to infrared wavelength. Due to the synergetic effect of nanosize, surface, phase transition, percolation threshold, and the band structure of the heterojunction, the transfer and transport of photogenerated carriers modulate the device performance. This study probes new chances of applying VO_2-semiconductor-based nanocomposites for broad spectral photodetectors.

1. INTRODUCTION

Photodetection has been applied to various applications, such as imaging,[1] remote sensing,[2] biological processes,[3] optical communication,[4] and target recognition.[5] However, photoelectronic materials in traditional photodetectors work for certain spectral bands, such as zinc oxide (ZnO) for ultraviolet (UV),[6] cadmium selenide (CdSe) for visible light,[7] and silicon (Si) for visible to near-infrared detection.[8] As a wide band gap semiconductor, ZnO is stable and has high carrier mobility, which can potentially improve the charge transport and enhance the device performance. In photovoltaic devices, ZnO films composed of ZnO nanocrystals (NCs) can serve as the electron transport layer.[9−12] In photodetectors, hybridization of ZnO with a second semiconductor, e.g., perovskite, could achieve an ambipolar photoresponse, higher switching ratio, faster response speed, and higher response and detection rate than compared to corresponding monophase devices.[13−16]

Vanadium dioxide (VO_2) is known as a functional material for smart windows,[17−20] infrared stealth,[21] imaging,[22] data storage,[23] memristors,[24] tunable-frequency metamaterials,[25] multifunctional sensors,[26,27] etc. It undergoes a reversible metal−insulator transition at ∼68 °C, which can be further lowered to room temperature by doping.[28−30] Monoclinic VO_2 (M) is a low-temperature phase, which is a semiconductor and infrared-transparent, whereas high-temperature rutile VO_2 (R) is a metal phase with low near-infrared transition and low infrared radiation. VO_2 is also used for infrared photodetectors, e.g., the high photoresponse of heterostructural VO_2/V_2O_5 nanobeams for 990 nm light,[31] VO_2 thin films prepared by the vapor transport method for 850 nm light,[32] and heavily hydrogen-doped VO_2 nanoparticles for 780 nm light.[33] The potential of VO_2 for a visible photodetector is also demonstrated, e.g., the use of tungsten-doped VO_2 single nanowires for photodetection under visible light excitation of 405, 532, and 660 nm.[34] Recently, Wadsley B phase VO_2(B) was found to have broad-band photodetection performances from the visible to terahertz region (405 nm to 0.88 mm).[35] However, studies on VO_2 for broad spectral photodetection covering the ultraviolet−visible−infrared (UV−Vis−IR) range are very limited.

In this report, a VO_2−ZnO composite nanomaterial system was investigated for broad spectral photodetectivity. The VO_2−ZnO composite was prepared by the NC-mist deposition strategy. The ZnO ratio, temperature, vacuum, and light

Received: April 24, 2022
Accepted: July 25, 2022
Published: October 13, 2022

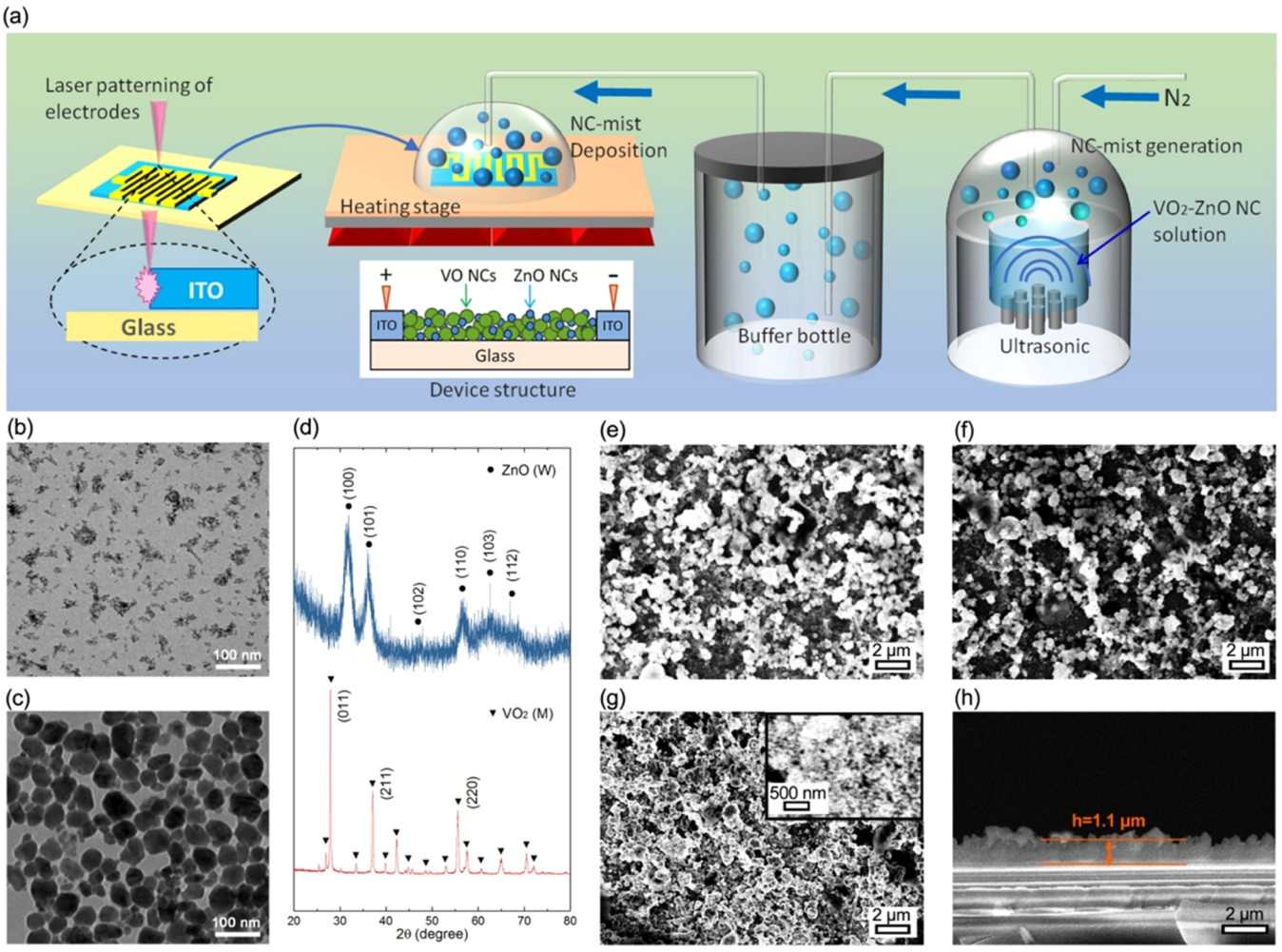

Figure 1. (a) Schematic illustration of the photodetector preparation and the device structure. TEM images of (b) ZnO nanocrystals and (c) VO_2 nanocrystals. (d) XRD patterns of ZnO and VO_2 nanocrystals. SEM images of (e) VO_2, (f) VO_2−10%ZnO, (g) and (h) VO_2−20%ZnO NC films.

wavelength-related performances were studied. An appropriate ZnO ratio would enhance the performance of the device compared with pure VO_2. It was found that not only the contribution from the single phase—such as the ultraviolet photodetectivity of ZnO or the near infrared photodetectivity of VO_2—works but also the NC surface and heterojunction band structure play important roles in the charge transfer and transport.

2. EXPERIMENTAL SECTION

2.1. Materials. NH_4VO_3 (99%), $N_2H_4{\cdot}H_2O$ (80%), HCl (98%), and HNO_3 (99.9%) were purchased from Aladdin Industrial Corporation. Zinc acetate dihydrate (99%), KOH (85%), *n*-butanol (99.5%), methanol (99.5%), and chloroform (99%) were bought from Sinopharm Chemical Reagent Co., Ltd. All of the chemicals were used without further purification.

2.2. Preparation of VO_2 NCs.[36,37] Typically, NH_4VO_3 (0.35 g) was added to deionized H_2O (70 mL) and stirred for 10 min. HCl (1.5 mL, 1 M) was added dropwise slowly until the solution turned orange and transparent. Then $N_2H_4{\cdot}H_2O$ (4.5 mL, 80%) was added, with the color changed from orange-yellow to dark green (in ∼5 min) and to wine red (in ∼8 min). After vigorous stirring for 4 h, the solution changed to turbid gray-green. The precipitate was collected by centrifugation. The collected precipitate was dispersed in H_2O (45 mL) and sonicated for 15 min. Then diluted HNO_3 (5.25 mL, 0.1 M) was added dropwise. After stirring for 4 h, the solution was sealed in a 100 mL autoclave and reacted at 240 °C for 36 h. The product was collected, dried, and thermal treated at 750 °C in an Ar gas atmosphere for 2 h to get the VO_2 NCs.

2.3. Synthesis of ZnO NCs.[38] Typically, zinc acetate dihydrate (3 g) was dissolved in methanol (150 mL) with stirring at 60 °C. A methanol solution of KOH (1.5 g, 65 mL) was added dropwise in 15 min. After 3 h of reaction with stirring, the solution was cooled down naturally. The ZnO NCs were collected by centrifugation (12 000 rpm) and washed twice with methanol. The ZnO NCs were dispersed in a solution of *n*-butanol−methanol−chloroform (volume ratio of 14:1:1) with a concentration of 6 mg/mL.

2.4. Device Fabrication and Measurements. The as-prepared VO_2 NCs were ground for 10 min in an agate mortar for further use. The ground VO_2 NCs (20 mg) were added to the ZnO NC solution in three ZnO proportions of 5, 10, and 20 wt %. The solution was diluted with H_2O to 75 mL and sonicated 1 min for device fabrication. The indium tin oxide (ITO) glass (15 Ω/□) was cleaned with acetone, ethanol, and deionized water. The interdigital electrodes were patterned by laser etching and acid washing of the ITO glass with a gap

https://doi.org/10.1021/acsomega.2c02549
ACS Omega 2022, 7, 37078−37084

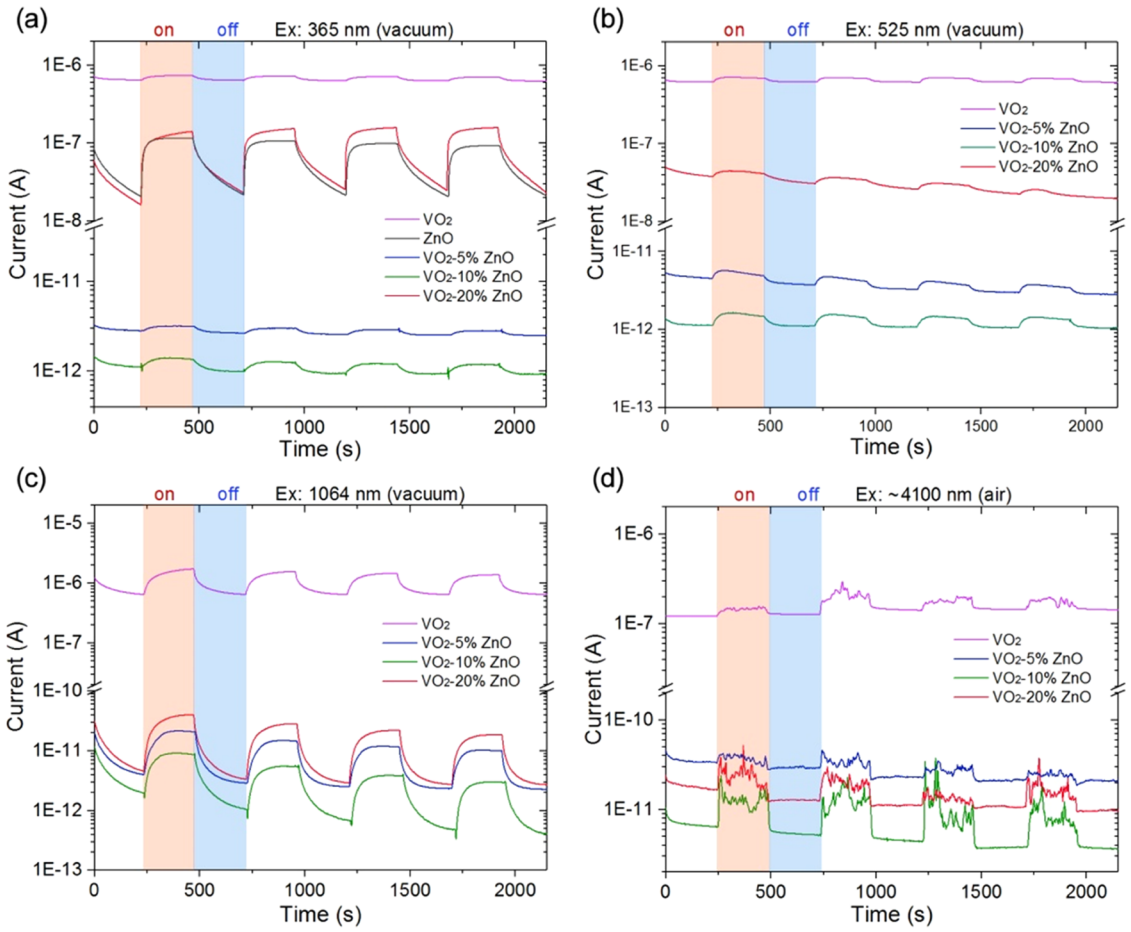

Figure 2. Photoresponse of VO_2, ZnO, and VO_2−ZnO devices under vacuum and 30 °C with excitation at (a) 365 nm, (b) 525 nm, (c) 1064 nm, and (d) ∼4100 nm.

width of 200 μm.[13,39] On a heating stage of 150 °C, the VO_2−ZnO NCs were deposited onto the ITO interdigital electrodes by the NC-mist deposition of the VO_2−ZnO NC solution, forming a lateral structured ITO/VO_2−ZnO NCs/ITO device. The photodetection properties were measured by a Keithley 2636B source meter. A diode of 365 nm and lasers of wavelengths of 365, 525, and 1064 nm with power values of 1.51, 2.11, and 3.02 mW/cm^2, respectively, were used as the ultraviolet−near infrared light sources. A heater at 700 K was used as the excitation source working at ∼4100 nm. The device working bias voltage was 10 V if not specifically mentioned. The switching ratio (SR) is calculated by

$$\mathrm{SR} = \frac{|I_{on} - I_{off}|}{I_{off}} \quad (1)$$

where I_{on} is the photocurrent and I_{off} is the dark current. The responsivity (R) defines the photocurrent generated per unit power of the incident light on the effective area of a photodetector and is calculated by

$$R = \frac{|I_{on} - I_{off}|}{P_{in}A} \quad (2)$$

where P_{in} is the light power and A is the effective area of the device. Detectivity (D^*) characterizes the detectable light level by the device and is given by

$$D^* = \frac{R}{\sqrt{\left(2e\frac{I_{off}}{A}\right)}} \quad (3)$$

Where e is the electronic charge and R is the responsivity of the device. Here, shot noise is used to calculate the detectivity, as the calculated value of Johnson noise is smaller, e.g., the values of shot noise and Johnson noise are 2.1×10^{-15} and 4.8×10^{-16} A for VO_2−20%ZnO, respectively.

2.5. Characterizations. The crystal structures of VO_2 and ZnO NCs were characterized by powder X-ray diffraction (XRD) with graphite-monochromatized Cu Kα radiation (λ = 0.15406 nm). The morphologies were characterized by transmission electron microscopy (TEM) using a JEM-200CX with an accelerating voltage of 80 kV and scanning electron microscopy (SEM) using JEOL JSM-7600F equipped with an energy-dispersive spectroscopy (EDS) system. The UV−Vis−IR spectra were measured by a Varian Cary 50 spectrophotometer. The energy band structures of the ZnO and VO_2 NCs were measured by ultraviolet photoelectron spectroscopy (UPS) using an EscaLab 250Xi. Differential scanning calorimetry (DSC) trace was recorded on a Diamond DSC instrument.

3. RESULTS AND DISCUSSION

The schematic illustration of the photodetector preparation is shown in Figure 1a. Because the VO_2 NCs used here are thermally treated at elevated temperature, the crystal surface is

https://doi.org/10.1021/acsomega.2c02549
ACS Omega 2022, 7, 37078−37084

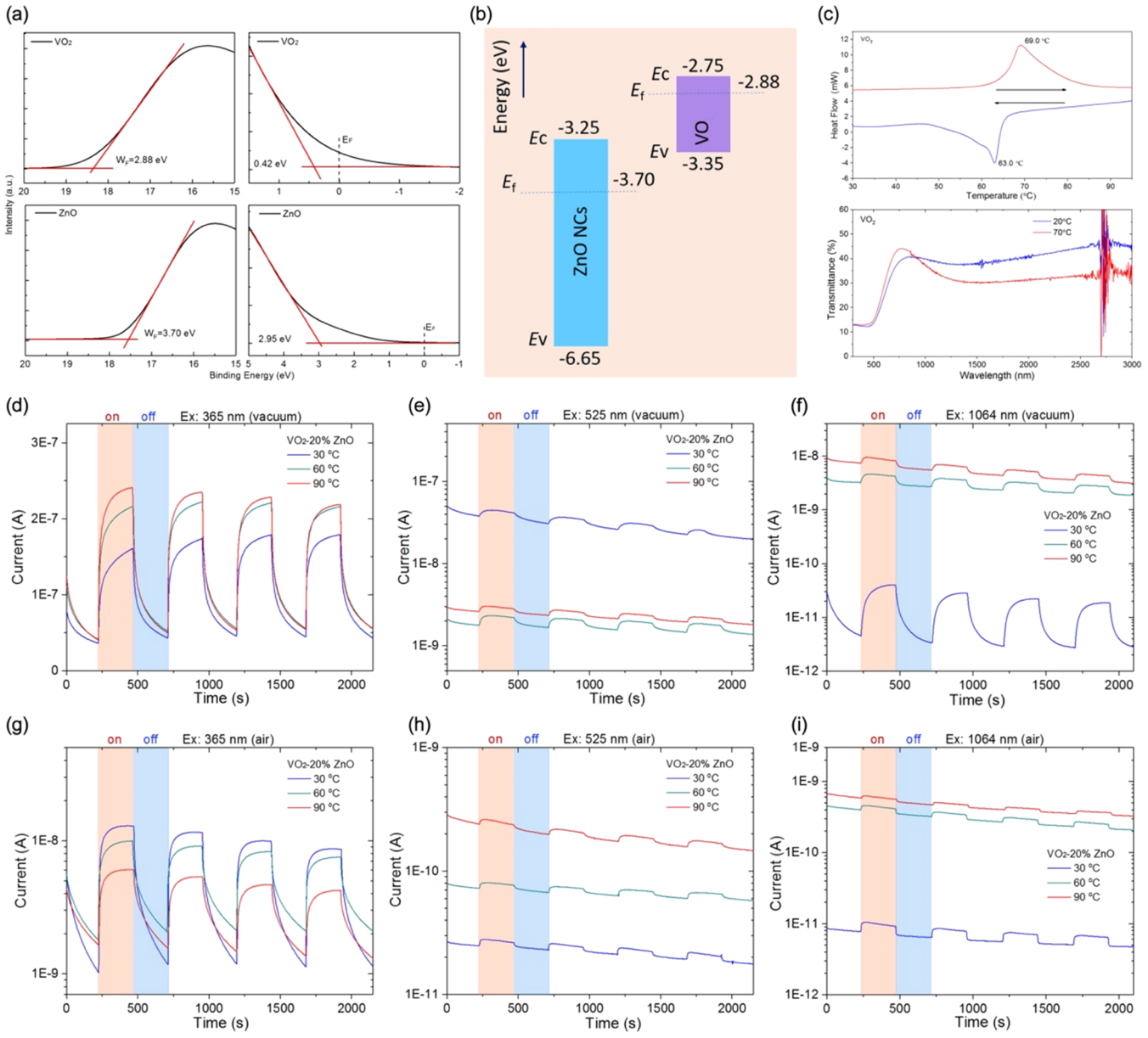

Figure 3. (a) UPS spectra of VO_2 and ZnO NCs. (b) Band structure of the VO_2−ZnO type-II heterojunction. (c) DSC curves (up) and temperature-dependent transmittance spectra of the VO_2 nanocrystals (below). Temperature-dependent photodetection performances of the VO_2−20%ZnO device with excitation at (d) 365 nm, (e) 525 nm, and (f) 1064 nm under vacuum and with excitation at (g) 365 nm, (h) 525 nm, and (i) 1064 nm in air.

clean without ligands. Their dispersion in solution is not as stable as ZnO NCs. Therefore, the common film preparation methods of spin-coating, dip-coating, and blade-coating are not applicable. Although introducing surfactants or soluble polymers as dispersing agents would help, their removal in the following steps would lead to the destruction of VO_2 or the film structure. To date, mist-assisted chemical deposition of functional thin films has been developed for ZnO, In_2O_3, and SnO_2 films used in solar cells, sensors, transistors, etc.[40−43] For the mist chemical deposition system, it is a challenge to prepare VO_2 films with phase purity.[44] To overcome this challenge, NC-containing mist-deposition is a newly developed technique and has been applied to prepare the GZO film.[45] Here, we use this method to prepare the VO_2−ZnO film. First, the VO_2−ZnO NC dispersion was atomized using an ultrasonic atomizer. The VO_2−ZnO NC-mist was carried by the N_2 flow to the substrate/electrodes on a heating stage. With an appropriate heating temperature (150 °C), the solvent of the mist evaporates quickly while depositing. At the same time, it will not lead to the degradation of the NCs. TEM characterization shows that the as-synthesized ZnO NCs are 3−5 nm and the VO_2 NCs are ∼50 nm on average (Figure 1b,c). XRD patterns (Figure 1d) indicate that the ZnO NCs are wurtzite structured (Joint Committee on Powder Diffraction Standards, JCPDS 89-7102) and VO_2 NCs are monoclinic structured (JCPDS 43-1051). The XRD pattern of the VO_2−20%ZnO film (Figure S1) shows the existence of VO_2 and ZnO feature peaks, suggesting their stability during the preparation. SEM images of the VO_2 and VO_2−ZnO NC films are shown in Figure 1e−g. Although these films are smooth macroscopically, they exhibit a porous feature on the nanometer scale. Due to the smaller size of ZnO NCs, the

https://doi.org/10.1021/acsomega.2c02549
ACS Omega 2022, 7, 37078−37084

pores between VO_2 NCs are gradually filled by the increased content of the ZnO NCs. The thickness of the film can be controlled by the deposition time. A typical lateral image of VO_2−20%ZnO film is shown in Figure 1h, exhibiting good uniformity of thickness ∼1.1 μm.

Figure 2 shows the photodetection performance of the devices based on films of VO_2 NCs containing 0, 5, 10, and 20% ZnO NCs. At all of these excitation wavelengths ranging from ultraviolet to the infrared, the device made using pure VO_2 NCs shows the highest dark current, suggesting the good conductivity. Under ultraviolet excitation, the VO_2−5%ZnO and VO_2−10%ZnO devices show 10^4−10^5 lower dark current than the pure VO_2, ZnO, and VO_2−20%ZnO devices.This observation is consistent with the fact that the dark current of the ZnO film is illumination history-dependent under ultraviolet excitation (Figure S2). It takes a long time of up to several hours for the dark current to drop down to the original dark current value range after illumination. A similar phenomenon was also reported in ZnO-based photodetectors.[46,47] It could be caused by the illumination-induced trapped charges in ZnO NCs.[48] Thus, the prolonged recombination time enhances the dark current value in a period after ultraviolet excitation. Therefore, the low dark current of the VO_2−5%ZnO and VO_2−10%ZnO could be mainly due to the disconnected nature of both VO_2 and ZnO. This is consistent with the fact that the VO_2−20%ZnO device has a comparable response to ZnO at 365 nm excitation because of the percolation effect. UPS spectra were measured to determine the band structures of the ZnO and VO_2 NCs (Figure 3a,b). It shows that VO_2−ZnO forms a type-II semiconductor heterojunction. The conduction band of VO_2 is higher than that of ZnO. Therefore, at low ZnO content, when excited by ultraviolet, the transport of photogenerated electrons in ZnO together with those transferred from the VO_2 would be confined in discrete ZnO, resulting in a low current. When the ZnO ratio is increased to 20%, the responsivity and photodetectivity are increased to 0.462 mA/W and 2.72×10^9 Jones, respectively, higher than 0.326 mA/W and 3.02×10^8 Jones for the pure VO_2 NC device and 0.353 mA/W and 1.84×10^9 Jones for the pure ZnO NC device. This suggests that 20% of ZnO exceeds the percolation threshold of the VO_2−ZnO nano composite, forming long-range connectivity of the ZnO NCs.

The performance of the device under visible light excitation at 525 nm, near-infrared at 1064 nm, and infrared at ∼4100 nm shares a similar behavior. The increased dark and light currents of VO_2−20%ZnO compared with those of VO_2−10% ZnO under visible-to-infrared excitation suggests the effective charge separation and positive contribution of ZnO to the current. The lower current of the nanocomposite than that of VO_2 is due to the segmentation effect of ZnO. Since ZnO has no absorption in these wavelengths, the photogenerated electrons are contributed by the VO_2 and transferred to ZnO. Although the responsivity and photodetectivity of the VO_2−ZnO devices for visible to near-infrared excitation are lower than the values of the pure VO_2 NC device, e.g., 10.1 mA/W and 4.19×10^9 Jones for the pure VO_2 NC device, which decreased to 3.29×10^{-4} mA/W and 5.21×10^9 Jones for the VO_2−20%ZnO device with excitation at 1064 nm, respectively. ZnO shows a positive contribution to the switching ratio. The switching ratio of the VO_2−20%ZnO device at 1064 nm is 8.95, higher than 2.68 of the pure VO_2 NC device. The enhancement of the switching ratio is also true for the ultraviolet and infrared excitations. It reaches 8.7 for the VO_2−20%ZnO device, higher than 1.14 for the pure VO_2 device and 4.46 for the pure ZnO device with 365 nm excitation. It is 2.12 for the VO_2-10%ZnO device, higher than 1.21 for the pure VO_2 device with ∼4100 nm excitation.

As VO_2 has a phase transition at 68 °C from the low-temperature M phase to the high-temperature R metallic phase (Figure 3c), it would be interesting to study the temperature-dependent photodetection. The temperature-dependent dark current of the VO_2−20%ZnO device was measured (Figure S3). It shows that the current remains almost unchanged before the M−R phase transition of VO_2, whereas it increases sharply around the phase transition point. As the excitation light power is too low to heat up the device reaching the phase transition point, the light-induced thermal effect has a negligible contribution to the responsivity of the device. Three temperatures of 30, 60, and 90 °C are selected to carry out the photodetection measurement of the VO2−20%ZnO device (Figure 3d−f). It is found that with the temperature increasing to 90 °C, the photodetectivity and switching ratio for ultraviolet excitation increased to 2.74×10^9 Jones and 5.91, respectively; photodetectivity increased from 6.91×10^6 Jones to 1.54×10^7 Jones and the switching ratio of 1.15 was almost unchanged for 525 nm excitation; and photodetectivity increased to 7.37×10^7 Jones and the switching ratio decreased to 1.28 for 1064 nm excitation. The excitation wavelength-dependent performance change with temperature is not surprising due to the phase change of VO_2 and different absorption ranges of ZnO and VO_2 NCs. It is noticed that the current increases with the temperature under the visible to near-infrared excitation, consistent with the VO_2 semiconductor to metallic phase transformation, suggesting that the charge carrier transport is possibly dominated by the hopping mechanism.[49−51] As shown in Figure 1, the VO_2−ZnO NC film prepared by the NC-mist deposition has a porous structure. The large specific surface is favorable to the adsorption of molecules in air such as H_2O, O_2, and CO_2, which would affect the photodetection. It shows that the current of the VO_2−20%ZnO device is lower in air than in vacuum (Figure 3g−i). However, the photodetectivity and switching ratio change trends are similar to those in vacuum except for the 365 nm excitation, which indicates that the adsorption states, especially the O_2 adsorption on ZnO surface defects, are sensitive to the ultraviolet light.[52−54] In a control experiment, a nonporous spin-coated film made using the same ZnO NCs shows much higher conductivity and an enhanced detectivity of 2.30×10^{11} Jones for 365 nm excitation (Figure S4). This suggests that the film structure significantly affects the device performance.

4. CONCLUSIONS

In summary, the potential of using VO_2−ZnO NCs for broad spectral photodetection was preliminarily investigated. Compared with the pure VO_2 device of the same structure, an enhanced switching ratio was achieved across the ultraviolet, visible, and infrared range. The nanosize of VO_2 and ZnO showed a prominent effect on the surface adsorption states and charge transport mechanism. The photodetectors exhibited temperature- and vacuum/air-dependent photoresponses. The band structure of the VO_2−ZnO system facilitates the electron transfer to the ZnO. Thus, the ZnO ratio regarding the percolation threshold in the composite is of critical importance to the device performance. Although the photodetectivity and

https://doi.org/10.1021/acsomega.2c02549
ACS Omega 2022, 7, 37078−37084

responsivity are not satisfactory for commercial applications at the present state, this study probes the possibility of utilizing VO_2-semiconductor-based nanocomposites for broad spectral photodetectors. Improvement could be expected by optimization of the material system, fabrication technique, and device structure.

■ ASSOCIATED CONTENT

Supporting Information

The Supporting Information is available free of charge at https://pubs.acs.org/doi/10.1021/acsomega.2c02549.

XRD pattern of the VO_2−20%ZnO film; photoresponse of the NC-mist deposited ZnO NC film; temperature dependent dark current of the VO_2−20%ZnO device in vacuum; photoresponse with ultraviolet excitation (PDF)

■ AUTHOR INFORMATION

Corresponding Author

Xiangxing Xu − *Jiangsu Key Laboratory of Biofunctional Materials, Jiangsu Key Laboratory of New Power Batteries, School of Chemistry and Materials Science, Nanjing Normal University, Nanjing 210046, P. R. China;* orcid.org/0000-0001-9135-9403; Email: xuxx@njnu.edu.cn

Authors

Danting Xu − *Jiangsu Key Laboratory of Biofunctional Materials, Jiangsu Key Laboratory of New Power Batteries, School of Chemistry and Materials Science, Nanjing Normal University, Nanjing 210046, P. R. China*

Xia Zhu − *Jiangsu Key Laboratory of Biofunctional Materials, Jiangsu Key Laboratory of New Power Batteries, School of Chemistry and Materials Science, Nanjing Normal University, Nanjing 210046, P. R. China*

Jiakun An − *Jiangsu Key Laboratory of Biofunctional Materials, Jiangsu Key Laboratory of New Power Batteries, School of Chemistry and Materials Science, Nanjing Normal University, Nanjing 210046, P. R. China*

Gaoyu Chen − *Jiangsu Key Laboratory of Biofunctional Materials, Jiangsu Key Laboratory of New Power Batteries, School of Chemistry and Materials Science, Nanjing Normal University, Nanjing 210046, P. R. China*

Jianchun Bao − *Jiangsu Key Laboratory of Biofunctional Materials, Jiangsu Key Laboratory of New Power Batteries, School of Chemistry and Materials Science, Nanjing Normal University, Nanjing 210046, P. R. China;* orcid.org/0000-0003-2818-6786

Complete contact information is available at: https://pubs.acs.org/10.1021/acsomega.2c02549

Author Contributions

†D.X. and X.Z. contributed equally to this work. The paper was completed by contributions of all of the authors. All of the authors approved the final version of the paper.

Notes

The authors declare no competing financial interest.

The authors declare that they have no known competing financial interests or personal relationships that could have appeared to influence the work reported in this paper.

■ ACKNOWLEDGMENTS

This work was financially supported by the National Natural Science Foundation of China (Nos. 21871143, 22175095, and 22075147).

■ REFERENCES

(1) Li, L.; Ye, S.; Qu, J.; Zhou, F.; Song, J.; Shen, G. Recent advances in perovskite photodetectors for image sensing. *Small* **2021**, *17*, No. 2005606.

(2) Refaat, T. F.; Abedin, M. N.; Bhagwat, V.; Bhat, I. B.; Dutta, P. S.; Singh, U. N. InGaSb photodetectors using an InGaSb substrate for 2 μm applications. *Appl. Phys. Lett.* **2004**, *85*, 1874−1876.

(3) Rezaei-Mazinani, S.; Ivanov, A. I.; Proctor, C. M.; Gkoupidenis, P.; Bernard, C.; Malliaras, G. G.; Ismailova, E. Monitoring intrinsic optical signals in brain tissue with organic photodetectors. *Adv. Mater. Technol.* **2018**, *3*, No. 1700333.

(4) Pospischil, A.; Humer, M.; Furchi, M. M.; Bachmann, D.; Guider, R.; Fromherz, T.; Mueller, T. CMOS-compatible graphene photodetector covering all optical communication bands. *Nat. Photonics* **2013**, *7*, 892−896.

(5) Xiong, J.; Li, F.; Zhao, N.; Jiang, N. Tracking and recognition of multiple human targets moving in a wireless pyroelectric infrared sensor network. *Sensors* **2014**, *14*, 7209−7228.

(6) Ning, Y.; Zhang, Z.; Teng, F.; Fang, X. Novel transparent and self-powered UV photodetector based on crossed ZnO nanofiber array homojunction. *Small* **2018**, *14*, No. 1703754.

(7) An, Q.; Meng, X.; Xiong, K.; Qiu, Y.; Lin, W. One-step synthesis of CdSe nanotubes with novel hollow tubular structure as high-performance active material for photodetector. *J. Alloys Compd.* **2017**, *726*, 214−220.

(8) Park, H.; Crozier, K. B. Vertically stacked photodetector devices containing silicon nanowires with engineered absorption spectra. *ACS Photonics* **2015**, *2*, 544−549.

(9) Li, S.; Zhang, P.; Wang, Y.; Sarvari, H.; Liu, D.; Wu, J.; Yang, Y.; Wang, Z.; Chen, Z. D. Interface engineering of high efficiency perovskite solar cells based on ZnO nanorods using atomic layer deposition. *Nano Res.* **2017**, *10*, 1092−1103.

(10) Bouhjar, F.; Derbali, L.; Mari, B. High performance novel flexible perovskite solar cell based on a low-cost-processed ZnO:Co electron transport layer. *Nano Res.* **2020**, *13*, 2546−2555.

(11) Chandrasekhar, P. S.; Dubey, A.; Qiao, Q. High efficiency perovskite solar cells using nitrogen-doped graphene/ZnO nanorod composite as an electron transport layer. *Sol. Energy* **2020**, *197*, 78−83.

(12) Chen, R.; Cao, J.; Duan, Y.; Hui, Y.; Chuong, T. T.; Ou, D.; Han, F.; Cheng, F.; Huang, X.; Wu, B.; Zheng, N. High-efficiency, hysteresis-less, uv-stable perovskite solar cells with cascade ZnO-ZnS electron transport layer. *J. Am. Chem. Soc.* **2019**, *141*, 541−547.

(13) An, J.; Chen, G.; Zhu, X.; Lv, X.; Bao, J.; Xu, X. Ambipolar photoresponse of $CsPbX_3$-ZnO (X = Cl, Br, and I) heterojunctions. *ACS Appl. Electron. Mater.* **2022**, *4*, 1525−1532.

(14) Li, H.; Liu, B.; Lin, W.; Liu, Y.; Wang, Y.; Zhang, Z.; Xiong, L.; Tao, J. Enhancing performance of broadband photodetectors based on perovskite $CsPbBr_3$ nanocrystals/ZnO-microwires heterostructures. *Sci. Adv. Mater.* **2021**, *13*, 1748−1755.

(15) Pan, X.; Zhang, J.; Zhou, H.; Liu, R.; Wu, D.; Wang, R.; Shen, L.; Tao, L.; Zhang, J.; Wang, H. Single-layer ZnO hollow hemispheres enable high-performance self-powered perovskite photodetector for optical communication. *Nano-Micro Lett.* **2021**, *13*, No. 70.

(16) Shao, D.; Zhu, W.; Xin, G.; Liu, X.; Wang, T.; Shi, S.; Lian, J.; Sawyer, S. A high performance UV−visible dual-band photodetector based on an inorganic Cs_2SnI_6 perovskite/ZnO heterojunction structure. *J. Mater. Chem. C* **2020**, *8*, 1819−1825.

(17) Cui, Y.; Ke, Y.; Liu, C.; Chen, Z.; Wang, N.; Zhang, L.; Zhou, Y.; Wang, S.; Gao, Y.; Long, Y. Thermochromic VO_2 for energy-efficient smart windows. *Joule* **2018**, *2*, 1707−1746.

(18) Vu, T. D.; Chen, Z.; Zeng, X.; Jiang, M.; Liu, S.; Gao, Y.; Long, Y. Physical vapour deposition of vanadium dioxide for thermochromic smart window applications. *J. Mater. Chem. C* **2019**, *7*, 2121−2145.
(19) Xu, F.; Cao, X.; Luo, H.; Jin, P. Recent advances in VO_2-based thermochromic composites for smart windows. *J. Mater. Chem. C* **2018**, *6*, 1903−1919.
(20) Liu, S.; Tso, C. Y.; Lee, H. H.; Du, Y. W.; Yu, K. M.; Feng, S.-P.; Huang, B. Self-densified optically transparent VO_2 thermochromic wood film for smart windows. *ACS Appl. Mater. Interfaces* **2021**, *13*, 22495−22504.
(21) Zhao, Y.; Fang, F. Thermochromism frequency-selective emitter for infrared stealth application. *ACS Appl. Electron. Mater.* **2021**, *3*, 2694−2702.
(22) Lang, F.; Wang, H.; Zhang, S.; Liu, J.; Yan, H. Review on variable emissivity materials and devices based on smart chromism. *Int. J. Thermophys.* **2018**, *39*, No. 6.
(23) Lee, M. J.; Park, Y.; Suh, D. S.; Lee, E. H.; Seo, S.; Kim, D. C.; Jung, R.; Kang, B. S.; Ahn, S. E.; Lee, C. B.; Seo, D. H.; Cha, Y. K.; Yoo, I. K.; Kim, J. S.; Park, B. H. Two series oxide resistors applicable to high speed and high density nonvolatile memory. *Adv. Mater.* **2007**, *19*, 3919−3923.
(24) Driscoll, T.; Kim, H. T.; Chae, B. G.; Di Ventra, M.; Basov, D. N. Phase-transition driven memristive system. *Appl. Phys. Lett.* **2009**, *95*, No. 043503.
(25) Driscoll, T.; Palit, S.; Qazilbash, M. M.; Brehm, M.; Keilmann, F.; Chae, B. G.; Yun, S. J.; Kim, H. T.; Cho, S. Y.; Jokerst, N. M.; Smith, D. R.; Basov, D. N. Dynamic tuning of an infrared hybrid-metamaterial resonance using vanadium dioxide. *Appl. Phys. Lett.* **2008**, *93*, No. 024101.
(26) Ke, Y.; Wang, S.; Liu, G.; Li, M.; White, T. J.; Long, Y. Vanadium dioxide: the multistimuli responsive material and its applications. *Small* **2018**, *14*, No. 1802025.
(27) Liao, F.; Lu, C.; Yao, G.; Yan, Z.; Gao, M.; Pan, T.; Zhang, Y.; Feng, X.; Lin, Y. Ultrasensitive flexible temperature-mechanical dual-parameter sensor based on vanadium dioxide Films. *IEEE Electron Device Lett.* **2017**, *38*, 1128−1131.
(28) Burkhardt, W.; Christmann, T.; Franke, S.; Kriegseis, W.; Meister, D.; Meyer, B. K.; Niessner, W.; Schalch, D.; Scharmann, A. Tungsten and fluorine co-doping of VO_2 films. *Thin Solid Films* **2002**, *402*, 226−231.
(29) Mlyuka, N. R.; Niklasson, G. A.; Granqvist, C. G. Mg doping of thermochromic VO_2 films enhances the optical transmittance and decreases the metal-insulator transition temperature. *Appl. Phys. Lett.* **2009**, *95*, No. 171909.
(30) Zhang, Y.; Zhang, J.; Zhang, X.; Deng, Y.; Zhong, Y.; Huang, C.; Liu, X.; Liu, X.; Mo, S. Influence of different additives on the synthesis of VO_2 polymorphs. *Ceram. Int.* **2013**, *39*, 8363−8376.
(31) Li, Z.; Hu, Z.; Peng, J.; Wu, C.; Yang, Y.; Feng, F.; Gao, P.; Yang, J.; Xie, Y. ultrahigh infrared photoresponse from core-shell single-domain-VO_2/V_2O_5 heterostructure in nanobeam. *Adv. Funct. Mater.* **2014**, *24*, 1821−1830.
(32) Guo, X.; Tan, Y.; Hu, Y.; Zafar, Z.; Liu, J.; Zou, J. High quality VO_2 thin films synthesized from V_2O_5 powder for sensitive near-infrared detection. *Sci. Rep.* **2021**, *11*, No. 21749.
(33) Kim, M. W.; Jo, Y. R.; Lee, C.; Moon, W. J.; Shim, J. H.; Kim, B. J. Ultrafast infrared photoresponse from heavily hydrogen-doped VO_2 single crystalline nanoparticles. *Nano Lett.* **2020**, *20*, 2733−2740.
(34) Lu, J.; Liu, H.; Deng, S.; Zheng, M.; Wang, Y.; van Kan, J. A.; Tang, S. H.; Zhang, X.; Sow, C. H.; Mhaisalkar, S. G. Highly sensitive and multispectral responsive phototransistor using tungsten-doped VO_2 nanowires. *Nanoscale* **2014**, *6*, 7619−7627.
(35) Zhang, Y.; Wang, X.; Zhou, Y.; Lai, H.; Liu, P.; Chen, H.; Wang, X.; Xie, W. Highly sensitive and ultra-broadband VO_2(B) photodetector dominated by bolometric effect. *Nano Lett.* **2022**, *22*, 485−493.
(36) Wu, C.; Zhang, X.; Dai, J.; Yang, J.; Wu, Z.; Wei, S.; Xie, Y. Direct hydrothermal synthesis of monoclinic VO_2(M) single-domain nanorods on large scale displaying magnetocaloric effect. *J. Mater. Chem.* **2011**, *21*, 4509−4517.
(37) Zhong, L.; Li, K.; Luo, Y.; Li, M.; Wang, H.; Li, G. Phase evolution of VO_2 polymorphs during hydrothermal treatment in the presence of AOT. *Cryst. Growth Des.* **2017**, *17*, 5927−5934.
(38) Liu, D.; Kelly, T. L. Perovskite solar cells with a planar heterojunction structure prepared using room-temperature solution processing techniques. *Nat. Photonics* **2014**, *8*, 133−138.
(39) He, Q.; Chen, G.; Wang, Y.; Liu, X.; Xu, D.; Xu, X.; Liu, Y.; Bao, J.; Wang, X. $CsPbX_3$-ITO (X = Cl, Br, I) nano-heterojunctions: voltage tuned positive to negative photoresponse. *Small* **2021**, *17*, No. 2101403.
(40) Zhou, Z. B.; Cui, R. Q.; Pang, Q. J.; Wang, Y. D.; Meng, F. Y.; Sun, T. T.; Ding, Z. M.; Yu, X. B. Preparation of indium tin oxide films and doped tin oxide films by an ultrasonic spray CVD process. *Appl. Surf. Sci.* **2001**, *172*, 245−252.
(41) Sawada, Y.; Kobayashi, C.; Seki, S.; Funakubo, H. Highly-conducting indium-tin-oxide transparent films fabricated by spray CVD using ethanol solution of indium (III) chloride and tin (II) chloride. *Thin Solid Films* **2002**, *409*, 46−50.
(42) Ogi, T.; Hidayat, D.; Iskandar, F.; Purwanto, A.; Okuyama, K. Direct synthesis of highly crystalline transparent conducting oxide nanoparticles by low pressure spray pyrolysis. *Adv. Powder Technol.* **2009**, *20*, 203−209.
(43) Shirahata, T.; Kawaharamura, T.; Fujita, S.; Orita, H. Transparent conductive zinc-oxide-based films grown at low temperature by mist chemical vapor deposition. *Thin Solid Films* **2015**, *597*, 30−38.
(44) Matamura, Y.; Ikenoue, T.; Miyake, M.; Hirato, T. Mist CVD of vanadium dioxide thin films with excellent thermochromic properties using a water-based precursor solution. *Sol. Energy Mater. Sol. Cells* **2021**, *230*, No. 111287.
(45) Nishi, Y.; Kasai, Y.; Suzuki, R.; Matsubara, M.; Muramatsu, A.; Kanie, K. Gallium-doped zinc oxide nanoparticle thin films as transparent electrode materials with high conductivity. *ACS Appl. Nano Mater.* **2020**, *3*, 9622−9632.
(46) Huang, J.; Lee, J.; Nakayama, H.; Schrock, M.; Cao, D. X.; Cho, K.; Bazan, G. C.; Nguyen, T.-Q. Understanding and countering illumination-sensitive dark current: toward organic photodetectors with reliable high detectivity. *ACS Nano* **2021**, *15*, 1753−1763.
(47) Zhou, X.; Yang, D.; Ma, D.; Vadim, A.; Ahamad, T.; Alshehri, S. M. Ultrahigh gain polymer photodetectors with spectral response from UV to near-infrared using ZnO nanoparticles as anode interfacial layer. *Adv. Funct. Mater.* **2016**, *26*, 6619−6626.
(48) Kim, H. H.; Lee, Y.; Lee, Y. J.; Jeong, J.; Yi, Y.; Park, C.; Yim, S.-Y.; Angadi, B.; Ko, K.-J.; Kang, J.-W.; Choi, W. K. Realization of excitation wavelength independent blue emission of ZnO quantum dots with intrinsic defects. *ACS Photonics* **2020**, *7*, 723−734.
(49) Gilmore, R. H.; Lee, E. M. Y.; Weidman, M. C.; Willard, A. P.; Tisdale, W. A. Charge carrier hopping dynamics in homogeneously broadened PbS quantum dot solids. *Nano Lett.* **2017**, *17*, 893−901.
(50) Liu, H.; Pourret, A.; Guyot-Sionnest, P. Mott and Efros-Shklovskii variable range hopping in CdSe quantum dots films. *ACS Nano* **2010**, *4*, 5211−5216.
(51) Gilmore, R. H.; Winslow, S. W.; Lee, E. M. Y.; Ashner, M. N.; Yager, K. G.; Willard, A. P.; Tisdale, W. A. Inverse temperature dependence of charge carrier hopping in quantum dot solids. *ACS Nano* **2018**, *12*, 7741−7749.
(52) Ma, H.; Liu, K.; Cheng, Z.; Zheng, Z.; Liu, Y.; Zhang, P.; Chen, X.; Liu, D.; Liu, L.; Shen, D. Speed enhancement of ultraviolet photodetector base on ZnO quantum dots by oxygen adsorption on surface defects. *J. Alloys Compd.* **2021**, *868*, No. 159252.
(53) Wang, Y.; Wang, P.; Zhu, Y.; Gao, J.; Gong, F.; Li, Q.; Xie, R.; Wu, F.; Wang, D.; Yang, J.; Fan, Z.; Wang, X.; Hu, W. High performance charge-transfer induced homojunction photodetector based on ultrathin ZnO nanosheet. *Appl. Phys. Lett.* **2019**, *114*, No. 011103.
(54) Zhu, Q.; Xie, C.; Li, H.; Zeng, D. A method for modeling and deciphering the persistent photoconductance and long-term charge storage of ZnO nanorod arrays. *Nano Res.* **2016**, *9*, 2972−3002.

https://doi.org/10.1021/acsomega.2c02549
ACS Omega 2022, 7, 37078−37084